

AC²L-GAD: Active Counterfactual Contrastive Learning for Graph Anomaly Detection

Kamal Berahmand

kamal.berahmand@rmit.edu.au
RMIT University
Melbourne, Victoria, Australia

Saman Forouzandeh

saman.forouzandeh@rmit.edu.au
RMIT University
Melbourne, Victoria, Australia

Mehrnoosh Mohammadi

m.mohammadibolbanabad@uq.edu.au
The University of Queensland
Brisbane, Queensland, Australia

Parham Moradi

parham.moradi@rmit.edu.au
RMIT University
Melbourne, Victoria, Australia

Mahdi Jalili

mahdi.jalili@rmit.edu.au
RMIT University
Melbourne, Victoria, Australia

Abstract

Graph anomaly detection aims to identify abnormal patterns in networks, but faces significant challenges from label scarcity and extreme class imbalance. While graph contrastive learning offers a promising unsupervised solution, existing methods suffer from two critical limitations: random augmentations break semantic consistency in positive pairs, while naive negative sampling produces trivial, uninformative contrasts. We propose AC²L-GAD, an Active Counterfactual Contrastive Learning framework that addresses both limitations through principled counterfactual reasoning. By combining information-theoretic active selection with counterfactual generation, our approach identifies structurally complex nodes and generates anomaly-preserving positive augmentations alongside normal negative counterparts that provide hard contrasts, while restricting expensive counterfactual generation to a strategically selected subset. This design reduces computational overhead by approximately 65% compared to full-graph counterfactual generation while maintaining detection quality. Experiments on nine benchmark datasets, including real-world financial transaction graphs from GADBench, show that AC²L-GAD achieves competitive or superior performance compared to state-of-the-art baselines, with notable gains in datasets where anomalies exhibit complex attribute-structure interactions.

Code: <https://anonymous.4open.science/r/AC2L-GAD-33B8>

Keywords

Graph anomaly detection, Contrastive learning, Counterfactual reasoning, Active learning

ACM Reference Format:

Kamal Berahmand, Saman Forouzandeh, Mehrnoosh Mohammadi, Parham Moradi, and Mahdi Jalili. 2026. AC²L-GAD: Active Counterfactual Contrastive Learning for Graph Anomaly Detection. In *Proceedings of the ACM Web Conference 2026 (WWW '26), April 13–17, 2026, Dubai, United Arab Emirates*. ACM, New York, NY, USA, 12 pages. <https://doi.org/10.1145/3774904.3792482>



This work is licensed under a Creative Commons Attribution-NonCommercial-NoDerivatives 4.0 International License.

WWW '26, Dubai, United Arab Emirates

© 2026 Copyright held by the owner/author(s).

ACM ISBN 979-8-4007-2307-0/2026/04

<https://doi.org/10.1145/3774904.3792482>

1 Introduction

Graph anomaly detection (GAD) is a fundamental task in network analysis, with applications in financial fraud prevention, cybersecurity, and biological network analysis. Following prior studies [15, 37], we focus on node-level anomaly detection. This task faces two key challenges: (i) the scarcity of labeled anomaly data, as obtaining reliable human annotations is costly and time-consuming, and (ii) severe class imbalance, where anomalies represent only a small fraction of instances while misclassification costs vary asymmetrically across applications. These constraints limit the applicability of supervised methods and have motivated growing interest in unsupervised approaches that leverage abundant unlabeled data [25, 37].

Within unsupervised GAD, graph contrastive learning (GCL) has emerged as the dominant paradigm. Unlike reconstruction-based approaches that suffer from ambiguous optimization objectives, unified latent spaces inadequate for diverse anomaly patterns, and high sensitivity to sparse attributes [3, 8, 22], GCL frameworks learn discriminative node embeddings by maximizing agreement between semantically consistent views while separating dissimilar views. This paradigm has proven effective across multiple domains [34, 38]. Recent specialized architectures have built on this foundation: CoLA [17] introduced node-subgraph contrast for local structural coherence, ANEMONE [12] incorporated multi-scale contrasts, and AD-GCL [32] explored anomaly-aware view construction and hard negative mining.

Despite these advances, existing GCL methods face two critical limitations. First, current approaches use stochastic augmentations—including random edge dropping, node removal, and feature masking—to construct positive pairs [4, 31, 34]. While effective for general representation learning, such augmentations lack semantic awareness: they apply uniform perturbations without considering local graph structure or anomaly-relevant patterns. Consequently, informative yet rare edges may be removed while spurious connections are retained, degrading semantic consistency and blurring boundaries between normal and abnormal nodes [11, 28]. We term this Gap G1: inconsistent positives due to random augmentation.

Second, negative sampling in existing methods typically relies on distance-based heuristics or uniform random selection [4, 6]. Such strategies produce trivial negatives that are easily separable from anchors, providing weak supervision and yielding coarse decision boundaries. This is particularly problematic in anomaly

detection, where anomalies often exhibit subtle deviations, hide within normal patterns, or concentrate in sparse regions [16, 33]. Without exposure to challenging negatives, models fail to develop the discriminative capacity required for accurate detection. We term this Gap G2: uninformative negatives from naive sampling.

These two gaps fundamentally limit the effectiveness of current GCL-based anomaly detection methods. Counterfactual reasoning offers a principled solution to both. Through minimal and controlled perturbations, counterfactual samples preserve semantic validity while introducing targeted variations. For positive pairs, counterfactuals preserve anomalous characteristics through controlled augmentations that maintain structural irregularity and attribute deviation, while for negatives, they normalize nodes by aligning features toward neighborhood centroids and increasing homophily with similar neighbors [33], thereby addressing inconsistent positives (Gap G1) and uninformative negatives (Gap G2). However, counterfactual generation is computationally expensive, typically requiring iterative gradient-based optimization for each node or subgraph [18, 19]. Applying this procedure graph-wide results in $O(|V|)$ complexity, making it impractical for large-scale networks.

To overcome this computational bottleneck, we introduce active counterfactual learning, where counterfactuals are generated only for a strategically selected subset of highly informative nodes. Drawing on principles from active learning [2, 9], we design a selection criterion combining structural complexity and attribute divergence to identify nodes that contribute most to representation quality. This reduces computational overhead from $O(|V|)$ to $O(k)$ where $k \ll |V|$, while maintaining—and often improving—model performance by focusing counterfactual generation on the most important training instances. This represents the first integration of active learning with counterfactual reasoning for graph anomaly detection.

We present AC²L-GAD (Active Counterfactual Contrastive Learning for Graph Anomaly Detection), a unified framework that addresses Gaps G1 and G2 through the combination of information-theoretic active selection and principled counterfactual generation. The framework integrates active node selection, counterfactual augmentation, graph encoding, contrastive optimization, and neighborhood-based anomaly scoring into a coherent pipeline, enabling both efficient training and accurate detection. Our contributions are threefold:

- We propose AC²L-GAD, a unified framework that integrates active learning with counterfactual reasoning to address two fundamental limitations in graph contrastive learning for anomaly detection: Gap G1 (inconsistent positives from random augmentation) and Gap G2 (uninformative negatives from naive sampling), achieving both representational quality and computational efficiency.
- We introduce an active counterfactual generation mechanism that combines information-theoretic node selection with principled counterfactual reasoning to generate anomaly-preserving positive augmentations and normalized hard negatives, reducing computational overhead by approximately 65% compared to full-graph counterfactual generation while maintaining detection quality.

- We conduct extensive experiments across nine benchmark datasets, including real-world financial fraud graphs from GADBench, demonstrating that AC²L-GAD achieves competitive or superior performance compared to eighteen state-of-the-art baselines, with notable improvements on datasets where anomalies exhibit complex attribute-structure interactions.

2 Related Work

Graph anomaly detection addresses the challenge of distinguishing abnormal nodes hidden among normal ones. Existing methods fall into three paradigms: traditional statistical approaches, reconstruction-based methods, and contrastive learning frameworks.

2.1 Traditional Graph Anomaly Detection

Traditional approaches rely on hand-crafted features and shallow heuristics. LOF [1] employs density-based estimation, comparing a node's local reachability density to that of its neighbors. AMEN [23] ranks anomalous attributed neighborhoods by jointly assessing structural consistency and attribute agreement in egonets. RADAR [14] formulates anomaly scoring as a regularized residual analysis over structure–attribute inconsistencies, while ANOMALOUS [21] jointly models structure and attributes to uncover deviations. GUIDE [35] leverages higher-order structural motifs (motif-degree) with a dual-autoencoder to reconstruct attributes and higher-order structures for unsupervised detection. While efficient and interpretable, these methods are limited by linear assumptions and manual feature engineering, and struggle with complex dependencies in high-dimensional attributed graphs, trading scalability and generalization for interpretability.

2.2 Reconstruction-based Methods

Reconstruction-based methods detect anomalies through reconstruction discrepancies, assuming that anomalous nodes are harder to reconstruct accurately due to their deviation from normal structural and attribute patterns. DOMINANT [3] first proposed a GCN-based autoencoder framework to jointly reconstruct attributes and topology. AnomalyDAE [8] utilizes a dual denoising autoencoder to enhance robustness against noisy features, while ALARM [22] adopts local reconstruction to capture fine-grained structural and attribute inconsistencies. ComGA [20] introduces community-aware reconstruction for topology–attribute alignment. ADA-GAD [10] employs an adaptive denoising mechanism that dynamically balances structural and attribute information. Finally, GAD-NR [26] performs neighborhood-level reconstruction using residual learning to improve sensitivity to local irregularities. Although these models effectively capture reconstruction errors, they remain sensitive to noise and often fail to generalize across diverse anomaly types.

2.3 Graph Contrastive Learning Methods

Graph contrastive learning has emerged as a powerful paradigm for unsupervised graph anomaly detection (GAD), aiming to learn representations that make normal node-context pairs similar and

abnormal ones dissimilar. CoLA [17] pioneered node-subgraph contrast, where a node and its RWR-sampled local subgraph form a positive pair. ANEMONE [12] extended this with a node-node branch to capture multi-scale structural and contextual irregularities. Subsequent works refined contrasting views and supervision: SubCR [36] decoupled local and global structures through intra-/inter-view contrast enhanced by attribute-consistency reconstruction, while GRADATE [7] introduced subgraph-subgraph contrast to strengthen representation robustness. More recently, AD-GCL [32] re-examined GCL-based anomaly detection from a structural imbalance perspective, proposing neighbor pruning for head nodes and anomaly-guided neighbor completion for tail nodes. In distributed settings, FedCAD [13] pioneered federated contrastive GAD via pseudo-labeled anomaly exchange and cross-client aggregation, while FedCLGN [30] improved privacy-preserving detection through global negative-pair pooling and local graph diffusion.

3 Preliminaries

3.1 Attributed Graph and Notation

We consider an *attributed graph* defined as $G = (V, E, X)$, where V is the set of $n = |V|$ nodes, E is the set of edges, and $X \in \mathbb{R}^{n \times d}$ is the node feature matrix with d -dimensional attributes for each node. The encoder f_θ maps nodes to low-dimensional embeddings that preserve both structural and attribute information. Table 1 summarizes the main symbols used throughout the paper.

Table 1: Summary of notations.

Symbol	Description
$G = (V, E, X)$	Attributed graph (nodes, edges, features)
$n = V $	Number of nodes
d	Feature dimension
$X \in \mathbb{R}^{n \times d}$	Node feature matrix
$f_\theta(\cdot)$	Graph encoder parameterized by θ
z_i	Embedding of node v_i
$S \subset V$	Selected subset ($ S = k$)
$\mathcal{H}_{\text{topo}}(v_i)$	Topology entropy
$\mathcal{D}(v_i)$	Attribute deviation
$c(v_i)$	Neighborhood consistency score
$a(v_i)$	Anomaly score in embedding space
x_i^+, x_i^-	Positive/negative <i>counterfactual</i> features
E_i^+, E_i^-	Positive/negative <i>counterfactual</i> edges
λ_u	Uniformity regularization weight

3.2 Unsupervised Graph Anomaly Detection

The objective of unsupervised GAD is to learn a scoring function

$$f : V \times G \rightarrow \mathbb{R},$$

that assigns each node $v_i \in V$ an anomaly score $f(v_i, G)$, where larger scores correspond to higher likelihoods of being anomalous. Unlike supervised methods, no anomaly labels are available during training, making the task highly challenging due to the scarcity of labeled anomalies and the extreme imbalance between normal and abnormal instances. Existing approaches either rely on reconstruction errors (e.g., autoencoders) or embedding deviations (e.g.,

consistency with local neighborhoods), both of which motivate our counterfactual-based formulation.

3.3 Graph Contrastive Learning

Graph Contrastive Learning (GCL) has emerged as a powerful paradigm for unsupervised representation learning on graphs [34]. It constructs augmented views of the same node or subgraph and maximizes their agreement while contrasting against negatives.

Given two augmentation distributions \mathcal{T}_1 and \mathcal{T}_2 , with $t_1(G) \sim \mathcal{T}_1(G)$ and $t_2(G) \sim \mathcal{T}_2(G)$, the standard InfoNCE objective is:

$$\mathcal{L}_{\text{GCL}} = - \sum_{i \in V} \log \frac{\exp(\text{sim}(z_i^{(1)}, z_i^{(2)})/\tau)}{\sum_{j \in V} \exp(\text{sim}(z_i^{(1)}, z_j^{(2)})/\tau)}, \quad (1)$$

where $z_i^{(m)} = f_\theta(t_m(G), v_i)$ is the embedding of node i under view m , and $\text{sim}(\cdot, \cdot)$ denotes the normalized dot product (cosine similarity). In practice, negatives are drawn from in-batch samples for scalability, rather than the entire graph.

3.4 Counterfactual Reasoning in Graphs

Counterfactual reasoning provides a principled framework for generating informative training samples through minimal, controlled perturbations [19, 29]. Given a node v_i with feature vector x_i and neighborhood $N(i)$, we define counterfactuals as minimal perturbations that alter the node's alignment with its local context, measured through a consistency score $c(v_i)$ (detailed in Section 4.2):

$$x_i^+ = \arg \min_{\Delta x} \|\Delta x\|_2 \quad \text{s.t.} \quad c(v_i + \Delta x) > \gamma \cdot c(v_i), \quad \gamma > 1, \quad (2)$$

$$x_i^- = \arg \min_{\Delta x} \|\Delta x\|_2 \quad \text{s.t.} \quad c(v_i + \Delta x) < \beta \cdot c(v_i), \quad \beta \in (0, 1). \quad (3)$$

Positive counterfactuals x_i^+ preserve anomalous characteristics by amplifying inconsistency with the neighborhood, while negative counterfactuals x_i^- normalize the node by reducing deviation toward its local context. This generates semantically similar positives and dissimilar hard negatives for effective contrastive learning.

4 Method: AC²L-GAD

We introduce AC²L-GAD (Active Counterfactual Contrastive Learning for Graph Anomaly Detection), an unsupervised framework that addresses two fundamental limitations in graph contrastive learning: (G1) random positive sampling that disrupts semantic consistency, and (G2) trivial negative sampling that provides weak supervision.

The framework integrates five modules into a unified pipeline (Fig. 1). Active node selection identifies structurally complex and attribute-divergent nodes to focus computational effort on anomaly-prone regions. Counterfactual augmentation generates positives that preserve anomalous characteristics through controlled variations and negatives that normalize nodes toward local patterns, creating effective anomaly-aware contrasts. A shared GCN encoder with lightweight projection heads processes original and counterfactual views. Contrastive optimization with uniformity regularization aligns anomalous anchors with their anomaly-preserving positives while separating them from normalized negatives. Finally, neighborhood-based scoring quantifies each node's deviation from its local context to produce anomaly scores.

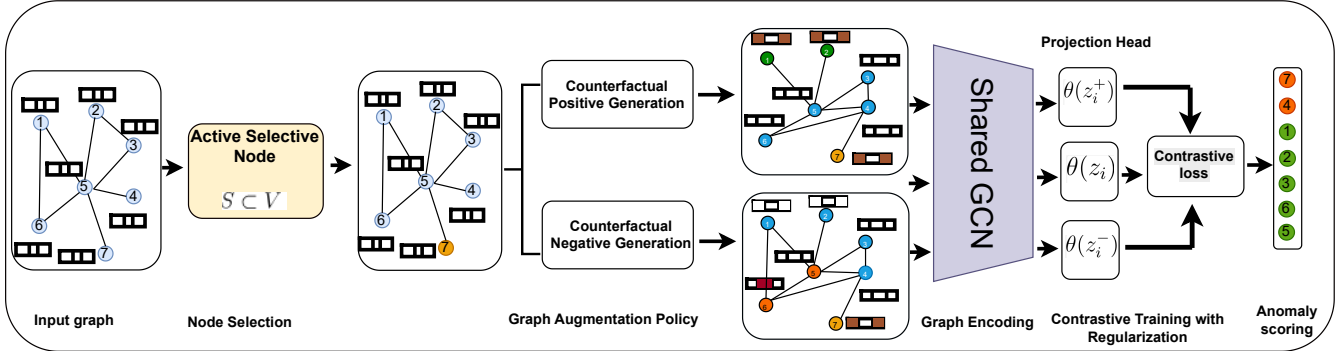


Figure 1: AC²L-GAD pipeline. The framework performs active node selection to focus on informative regions, generates anomaly-preserving counterfactual positives and normalized counterfactual negatives, and encodes original and augmented views with a shared GCN. A contrastive objective with uniformity regularization shapes the embedding space, from which anomaly scores are derived.

4.1 Active Node Selection via Structural and Attribute Criteria

As a preparatory step for *adaptive* augmentation, AC²L-GAD restricts augmentation to a *subset* of nodes rather than the entire graph. Concretely, we select a subset $S \subset V$ with $|S| = k$ and $k \ll |V|$, so that training focuses on anomaly-relevant regions and the per-epoch augmentation/sampling cost drops from $O(|V|)$ to $O(k)$. We set $k = \max(100, \lfloor 0.1|V| \rfloor)$ to balance efficiency and coverage. This design follows the *active learning* principle that most informative signal typically concentrates in a small number of *hard and diverse* samples; hence, operating on S provides a stronger supervision signal for downstream contrastive learning at a fraction of the cost.

Structural Complexity via Local Topology Entropy. We introduce a novel measure of structural informativeness that quantifies the heterogeneity of local patterns in a node’s neighborhood. For node v_i , we discretize structural indicators of its neighbors (degree, clustering coefficient, triangle count) into $B = 5$ bins based on graph-wide quantiles, and define:

$$\mathcal{H}_{\text{topo}}(v_i) = - \sum_{b \in B} p(b | v_i) \log p(b | v_i), \quad (4)$$

where $p(b | v_i)$ is the normalized frequency of pattern b among neighbors of v_i . A high entropy value indicates a structurally complex and informative local topology.

Attribute Deviation. To complement structural information, we also consider nodes whose attributes strongly deviate from their neighborhood. For node v_i with feature vector \mathbf{x}_i (where all features in X are z-score normalized), we compute:

$$\mathcal{D}(v_i) = \frac{\|\mathbf{x}_i - \bar{\mathbf{x}}_{N(i)}\|_2}{\sigma(\{\mathbf{x}_j : j \in N(i)\}) + \epsilon}, \quad (5)$$

where $\bar{\mathbf{x}}_{N(i)}$ and $\sigma(\cdot)$ denote the mean and standard deviation of neighbor features, respectively, and $\epsilon = 10^{-6}$ is a small constant for numerical stability. Large values signal attribute-level anomalies at decision boundaries.

4.1.1 Final Selection Rule. We select the top- $k/2$ nodes ranked by $\mathcal{H}_{\text{topo}}$ and the top- $k/2$ nodes ranked by \mathcal{D} , and take their union as S , resulting in $|S| \leq k$ nodes (with $|S| = k$ when the sets are disjoint). This procedure runs in $O(|V|dd)$ time and is executed once before training. The dual criterion is robust: entropy favors structurally heterogeneous regions, while deviation highlights attribute-level boundaries. In our ablation study we further validate the individual and union-based contributions of the two criteria.

4.2 Active Counterfactual Generation

Counterfactual augmentation is applied only to the informative subset S identified in the previous step. Unlike conventional methods that randomly sample negatives, our approach synthesizes counterfactuals that maintain anomalous patterns for positive pairs and normalize nodes for negative pairs, eliminating dependence on ground-truth labels while providing hard, informative contrasts. This directly tackles random positives (G1) and trivial negatives (G2).

Following the counterfactual framework introduced in Section 3.4, we generate positive and negative counterfactuals for each node in S through constrained optimization.

4.2.1 Feature Counterfactuals. We formalize counterfactual generation as constrained optimization problems that balance minimal perturbation with sufficient change in neighborhood consistency. To measure consistency, we define a combined score integrating attribute deviation and structural alignment:

$$c(v_i) = \lambda_{\text{attr}} \cdot \frac{\|\mathbf{x}_i - \bar{\mathbf{x}}_{N(i)}\|_2}{\sigma_{N(i)} + \delta} + \lambda_{\text{struct}} \cdot \left(1 - \frac{|N(i) \cap N_{\text{sim}}(i)|}{|N(i)|}\right), \quad (6)$$

where $\bar{\mathbf{x}}_{N(i)} = \frac{1}{|N(i)|} \sum_{j \in N(i)} \mathbf{x}_j$ is the neighbor feature centroid, $\sigma_{N(i)}$ denotes neighborhood standard deviation, $N_{\text{sim}}(i) = \{j \in N(i) : \cos(\mathbf{x}_i, \mathbf{x}_j) > 0.7\}$ identifies feature-similar neighbors (threshold chosen empirically), $\lambda_{\text{attr}} + \lambda_{\text{struct}} = 1$, and $\delta = 10^{-6}$ ensures numerical stability. Higher scores indicate greater inconsistency. We set $\lambda_{\text{attr}} = 0.8$ and $\lambda_{\text{struct}} = 0.2$, prioritizing attribute-based consistency as it proved more informative in preliminary validation.

Positive Counterfactuals. The ideal positive counterfactual solves:

$$x_i^+ = \arg \min_{x'} \|x_i - x'\|_2 \quad \text{s.t.} \quad c(v'_i) \geq \gamma \cdot c(v_i), \quad \gamma = 1.3. \quad (7)$$

Since exact optimization is intractable due to the non-convex nature of $c(\cdot)$, we employ a gradient-based approximation. Since the first term of $c(v_i)$ (attribute deviation) dominates with $\lambda_{\text{attr}} = 0.8$, moving away from the neighbor centroid effectively increases $c(v_i)$:

$$x_i^+ = x_i - \alpha_{\text{pos}} \cdot \frac{\bar{x}_{N(i)} - x_i}{\|\bar{x}_{N(i)} - x_i\|_2 + \delta}, \quad (8)$$

where $\alpha_{\text{pos}} = \min(0.3, (\gamma - 1) \cdot \frac{\|x_i - \bar{x}_{N(i)}\|_2}{0.5 \cdot \text{std}(X)})$ is an adaptive step size proportional to the current distance from the centroid, with maximum bound 0.3 to prevent excessive perturbations. We verify $c(v_i^+) > c(v_i)$ and $\|x_i - x_i^+\|_2 \leq 0.5 \cdot \text{std}(X)$; if violated, we scale α_{pos} by 0.5 iteratively (maximum 5 iterations). If constraints cannot be satisfied, we retain the original x_i as a fallback positive (maintaining the anchor's anomalous features without perturbation).

Negative Counterfactuals. Similarly, negative counterfactuals are generated by:

$$x_i^- = \arg \min_{x'} \|x_i - x'\|_2 \quad \text{s.t.} \quad c(v'_i) \leq \beta \cdot c(v_i), \quad \beta = 0.7, \quad (9)$$

with gradient-based approximation moving toward the neighbor centroid:

$$x_i^- = x_i + \alpha_{\text{neg}} \cdot \frac{\bar{x}_{N(i)} - x_i}{\|\bar{x}_{N(i)} - x_i\|_2 + \delta}, \quad (10)$$

where $\alpha_{\text{neg}} = \min(0.3, (1 - \beta) \cdot \frac{\|x_i - \bar{x}_{N(i)}\|_2}{0.5 \cdot \text{std}(X)})$ follows the same adaptive principle. We verify $c(v_i^-) < c(v_i)$ and perturbation bounds, applying iterative scaling if needed (maximum 5 iterations). If constraints cannot be satisfied, we discard the negative sample and rely on in-batch negatives during contrastive training. Empirical validation of approximation quality, constraint satisfaction rates, and failure mode analysis are provided in Appendix B.1.

4.2.2 Structural Counterfactuals. In addition to feature modifications, we adjust the local graph structure to enhance counterfactual quality. Positive structural counterfactuals aim to decrease homophily by connecting the node to dissimilar neighbors or removing connections to similar ones:

$$E_i^+ = \arg \min_{E'} |E_i \Delta E'| \quad \text{s.t.} \quad \text{homophily}(v_i, E') < \text{homophily}(v_i, E_i), \quad (11)$$

where E_i denotes the set of edges incident to node v_i , $E_i \Delta E'$ denotes their symmetric difference, and

$$\text{homophily}(v_i, E) = \frac{|\{j \in N_E(i) : \cos(x_i, x_j) > 0.7\}|}{|N_E(i)|} \quad (12)$$

measures the fraction of feature-similar neighbors under edge set E . Negative structural counterfactuals increase homophily:

$$E_i^- = \arg \min_{E'} |E_i \Delta E'| \quad \text{s.t.} \quad \text{homophily}(v_i, E') > \text{homophily}(v_i, E_i). \quad (13)$$

Since exact optimization is NP-hard, we employ a greedy heuristic: for positive counterfactuals, we iteratively remove up to 2 edges to feature-similar neighbors while optionally adding 1 edge to dissimilar 2-hop neighbors, ensuring degree change ≤ 2 and decreased homophily. For negative counterfactuals, we add up to 2 edges to

similar 2-hop neighbors and remove 1 dissimilar edge. The algorithm terminates when constraints are satisfied or no valid modifications remain. Detailed pseudocode and approximation analysis are in Appendix B.2.

The combined counterfactual for node v_i integrates both feature and structural modifications: $v_i^+ = (x_i^+, E_i^+)$ and $v_i^- = (x_i^-, E_i^-)$. During GCN encoding, we create node-specific views where each $v_i \in S$ uses feature vector x_i^\pm and a locally modified adjacency matrix in which edges incident to v_i are updated according to E_i^\pm while all other edges remain unchanged. Combined quality metrics demonstrating the complementary strengths of feature and structural counterfactuals are presented in Appendix B.3.

4.3 Graph Encoding and Projection Head

We encode original and counterfactual views using a shared 2-layer GCN encoder:

$$H^{(1)} = \text{ReLU}(\hat{A}XW^{(0)}), \quad (14)$$

$$Z = \hat{A}H^{(1)}W^{(1)}, \quad (15)$$

where $W^{(0)}, W^{(1)}$ are trainable weight matrices with dimensions $d \times 64$ and 64×32 respectively. For each node $v_i \in S$, we generate three embeddings using view-specific adjacency matrices: z_i (original graph A), z_i^+ (modified graph with edges E_i^+), and z_i^- (modified graph with edges E_i^-). A two-layer MLP projection head maps embeddings to the contrastive space: $h = \text{ReLU}(zW_p^{(1)})W_p^{(2)}$, where $W_p^{(1)} \in \mathbb{R}^{32 \times 64}$ and $W_p^{(2)} \in \mathbb{R}^{64 \times 32}$. All embeddings are ℓ_2 -normalized before computing similarities.

4.4 Contrastive Training with Regularization

For each anchor node $i \in S$, we construct positive and negative pairs using counterfactual embeddings. The positive is the counterfactual embedding z_i^+ , while negatives include the counterfactual negative z_i^- and in-batch anchors $\mathcal{B}_i = \{z_j : j \in S, j \neq i\}$.

4.4.1 InfoNCE Loss. The contrastive objective for anchor i is:

$$\ell_i = -s_i^+ + \log \left(e^{s_i^+} + \sum_{j \in \mathcal{B}_i} e^{s_{ij}} + e^{s_i^-} \right), \quad (16)$$

where $s_{ij} = z_i^\top z_j / \tau$ with $\tau = 0.1$ and ℓ_2 -normalized embeddings. The counterfactual negative z_i^- provides harder contrasts than random sampling.

4.4.2 Uniformity Regularization. To prevent representation collapse, we adopt the uniformity regularizer:

$$\mathcal{L}_{\text{unif}} = \log \left(\frac{1}{|S|(|S| - 1)} \sum_{i \neq j, i, j \in S} e^{-2\|z_i - z_j\|_2^2} \right), \quad (17)$$

which penalizes excessive concentration of embeddings. The weight λ_u is set based on graph sparsity: $\lambda_u = 0.05$ for dense graphs ($|E|/|V| \geq 3$) and $\lambda_u = 0.1$ for sparse graphs.

4.4.3 Overall Objective. The final loss combines contrastive and uniformity terms:

$$\mathcal{L} = \sum_{i \in S} \ell_i + \lambda_u \mathcal{L}_{\text{unif}}. \quad (18)$$

Algorithm 1 AC²L-GAD Training Pipeline

Require: Graph $G = (V, E, X)$, encoder f_θ , epochs T , budget k , learning rate η
Ensure: Trained encoder f_θ

- 1: $S \leftarrow \text{ACTIVESELECTION}(G, k)$ ▷ Once before training
- 2: **for** $t = 1$ to T **do**
- 3: **for** each $v_i \in S$ **do**
- 4: $(x_i^+, E_i^+), (x_i^-, E_i^-) \leftarrow \text{GENERATECF}(G, v_i)$
- 5: **end for**
- 6: $\{z_i, z_i^+, z_i^-\}_{i \in S} \leftarrow f_\theta(G, S)$ ▷ Encode with modified adjacency
- 7: $\mathcal{L} \leftarrow \sum_{i \in S} \ell_i + \lambda_u \mathcal{L}_{\text{unif}}$ ▷ Eqs. 12-14
- 8: $\theta \leftarrow \text{Adam}(\theta, \nabla_\theta \mathcal{L}, \eta)$
- 9: **end for**
- 10: **return** f_θ

4.4.4 Training Pipeline. We train using Adam optimizer with learning rate $\eta = 0.001$ for maximum $T = 200$ epochs. Early stopping (patience = 20) is applied based on contrastive loss convergence on a held-out validation set.

4.5 Neighborhood-Based Anomaly Scoring

After training, we perform anomaly detection in the learned embedding space. For each node $v_i \in V$, we compute its anomaly score as the deviation from its neighborhood centroid:

$$a(v_i) = \left\| z_i - \frac{1}{|N(i)|} \sum_{j \in N(i)} z_j \right\|_2, \quad (19)$$

where $z_i = f_\theta(v_i)$ is the final embedding produced by the trained encoder. This formulation mirrors the consistency score $c(v_i)$ from Equation 4, but operates in the learned embedding space where counterfactual-aware representations better capture anomaly-relevant deviations. For isolated nodes ($|N(i)| = 0$), we set $a(v_i) = \|z_i\|_2$.

Nodes are ranked by $a(v_i)$ in descending order, and the top- m nodes are flagged as anomalies, where m is determined by the expected anomaly ratio or detection budget. Unlike reconstruction-based methods that rely on proxy tasks (attribute/structure reconstruction), our approach directly optimizes embeddings for discriminative contrast between normal and abnormal patterns through counterfactual reasoning, yielding more reliable anomaly scores.

5 Experiments

We conduct comprehensive experiments to address the following research questions:

RQ1: Overall Detection Performance. How does AC²L-GAD compare to state-of-the-art methods across diverse graph types and anomaly patterns?

RQ2: Counterfactual Effectiveness. Do counterfactuals effectively address inconsistent positives (Gap G1) and uninformative negatives (Gap G2), providing higher semantic consistency and harder contrasts than random augmentation?

RQ3: Computational Efficiency. What is the performance-efficiency tradeoff of active selection compared to full-graph counterfactual generation?

RQ4: Robustness Analysis. How does performance degrade under feature noise and structural perturbations?

RQ5: Component Contributions. Which components (feature vs structural counterfactuals, active selection criteria, uniformity regularization) contribute most to overall performance?

5.1 Experimental Setup

Datasets. We evaluate on nine attributed graphs spanning three categories: (i) *ground-truth labeled*: Amazon and Enron contain real anomaly labels; (ii) *injected anomalies*: for Cora, Citeseer, Flickr, ACM, and Pubmed we inject structural and attribute anomalies following the protocol of [3] (randomly rewire 50% of edges and add Gaussian noise $\mathcal{N}(0, 0.5^2)$ with 30% feature masking); and (iii) *real-world GADBench*: T-Finance (39K nodes, 21M edges) and DGraph-Fin (3.7M nodes, 4.3M edges) are large-scale financial transaction graphs from the GADBench benchmark [27] containing real-world fraud patterns. Both datasets provide million-scale evaluation with lower anomaly ratios (1.3–4.6%) compared to injected datasets (3–6%), presenting more challenging detection scenarios. Many baselines fail to scale on these large graphs due to memory and computational constraints. Detailed dataset statistics are in Appendix A.

Baselines. We compare AC²L-GAD against 18 representative methods across three categories:

Traditional: ANOMALOUS [21], Radar [14], GUIDE [35].

Reconstruction-based: DOMINANT [3], AnomalyDAE [8], ComGA [20], ADA-GAD [10], GAD-NR [26], ALARM [22].

Contrastive-based: CoLA [17], ANEMONE [12], Sub-CR [36], GRADATE [7], FedCAD [13], FedCLGN [30], AD-GCL [32], TAM [24], SmoothGNN [5].

TAM (Truncated Affinity Maximization) models one-class homophily for anomaly detection, while SmoothGNN applies smoothing-aware graph neural networks specifically designed for financial fraud detection.

Implementation details. The encoder is a 2-layer GCN with hidden dimension 64 and output dimension 32, followed by a 2-layer MLP projection head (32 → 64 → 32). Training uses Adam optimizer with learning rate 0.001, weight decay 5×10^{-4} , and batch size 512. AC²L-GAD-specific parameters: temperature $\tau = 0.1$, uniformity weight $\lambda_u = 0.05$ for dense graphs ($|E|/|V| \geq 3$) and $\lambda_u = 0.1$ for sparse graphs, active selection budget $k = \max(100, \lfloor 0.1|V| \rfloor)$, counterfactual thresholds $\beta = 0.7$ and $\gamma = 1.3$, consistency weights $\lambda_{\text{attr}} = 0.8$ and $\lambda_{\text{struct}} = 0.2$. Early stopping (patience 20) monitors contrastive loss on a held-out validation set (10% of nodes). Anomaly labels are used *only for final evaluation*, never for training or hyperparameter selection. All experiments run on NVIDIA V100 GPUs (32GB), with results averaged over 10 independent runs.

Evaluation metrics. We report AUC-ROC and F1-score. F1 is computed at the threshold selecting top- m nodes, where m equals the true number of anomalies.

5.2 RQ1. Effectiveness

Table 2 compares AC²L-GAD against 18 baselines across nine datasets. AC²L-GAD achieves best or second-best performance on all datasets, with notable improvements on ACM (89.4% AUC, 74.7% F1) and Pubmed (97.2% AUC, 87.9% F1), outperforming AD-GCL by 4.3% AUC and 8.4% F1 on ACM. Compared to traditional,

reconstruction-based, and contrastive baselines, we achieve 15–25%, 3–8%, and 1–8% improvements respectively, validating that counterfactual generation addresses inconsistent positives (Gap G1) and uninformative negatives (Gap G2).

On real-world GADBench datasets, AC²L-GAD demonstrates effective generalization and scalability. On T-Finance (39K nodes, 21M edges, 4.58% anomaly ratio), we achieve 73.1% AUC and 53.1% F1, competitive with SmoothGNN (75.5% AUC, 58.5% F1). On DGraph-Fin (3.7M nodes, 4.3M edges, 1.27% anomaly ratio), we achieve 66.9% AUC and 55.4% F1, outperforming SmoothGNN (64.9% AUC) and ADA-GAD (66.2% AUC). The active selection mechanism enables practical deployment on million-node graphs, completing training in 4.2 hours on 4×V100 GPUs (28GB/GPU), while many baselines fail to scale (missing results in Table 2). The smaller performance gap on financial datasets (vs citation networks) reflects more challenging scenarios with camouflaged anomalies and significantly lower anomaly ratios (1.3–4.6% vs 3–6%).

The improvements are particularly pronounced on datasets with complex attribute-structure interactions (ACM, Pubmed), while remaining competitive on simpler datasets (Amazon, Enron), demonstrating broad generalization across diverse scales (1K–3.7M nodes, 3K–21M edges).

5.3 RQ2. Counterfactual Quality

To validate counterfactual effectiveness, we evaluate three quality metrics on the Cora dataset: (i) positive similarity $\text{sim}(z_i, z_i^+)$ measuring semantic preservation, (ii) negative margin $\|z_i - z_i^-\|_2$ quantifying separation, and (iii) neighborhood preservation (Jaccard similarity between original and counterfactual-positive neighborhoods) capturing structural coherence.

Table 3 compares AC²L-GAD against three augmentation baselines: random edge/feature perturbation, degree-based edge sampling, and Gaussian feature noise. Our method achieves substantially higher positive similarity (0.847 vs 0.721–0.763), larger negative margins (1.34 vs 0.98–1.12), and better neighborhood preservation (78.3% vs 52.1–61.4%), demonstrating that counterfactual generation produces semantically consistent positives and informative hard negatives while maintaining structural validity. These improvements directly address Gap G1 (inconsistent positives) and Gap G2 (uninformative negatives).

Component-wise ablation (Table 5) shows that combining feature and structural counterfactuals yields 93.1% AUC on Cora, outperforming feature-only (92.3%) or structural-only (91.8%) approaches, confirming their complementary contributions.

5.4 RQ3. Efficiency and Computational Complexity

Counterfactual generation is computationally expensive when applied to all nodes. We demonstrate that active selection of $k = 10\%$ informative nodes preserves detection quality while achieving practical efficiency.

Per-epoch complexity for full counterfactual generation is $O(|V|\bar{d}^2 + |E|dh)$, where \bar{d} is average node degree and $h = 64$ is hidden dimension. Active selection reduces this to $O(k\bar{d}^2 + |E|dh)$ with $k = 0.1|V|$, yielding theoretical 10× reduction in counterfactual cost. The one-time selection overhead is $O(|V|d\bar{d})$.

Table 4 compares runtime and memory across three strategies on three datasets. On Pubmed (19.7K nodes), full counterfactual generation requires 127.8s/epoch and 28.5GB memory, while AC²L-GAD achieves 45.2s/epoch and 9.8GB (65% and 66% reduction) with no quality loss (97.2% AUC). Compared to random augmentation, we incur only 23% runtime and 24% memory overhead while achieving superior detection performance (97.2% vs 93.0% AUC), demonstrating a favorable quality-efficiency tradeoff. Memory scales linearly with graph size, remaining practical for graphs up to 20K nodes.

5.5 RQ4. Robustness

We evaluate stability under data corruption on Cora by introducing simulated perturbations. Feature noise adds Gaussian noise $\mathcal{N}(0, \sigma^2)$ with $\sigma \in \{0, 0.05, 0.1, 0.15, 0.2\}$ to node attributes. Structural noise randomly flips edges at rates $\rho \in \{0\%, 5\%, 10\%, 15\%, 20\%\}$. All results are averaged over 10 runs.

Figure 2 shows performance degradation curves under increasing noise levels. Under maximum feature corruption ($\sigma = 0.2$), AC²L-GAD retains 87.5% AUC (94% of clean performance), while ANEMONE degrades to 78.3% (86% retention) and Sub-CR to 73.2% (81% retention). Under 20% structural noise, AC²L-GAD achieves 84.3% AUC compared to 75.2% for ANEMONE and 69.8% for Sub-CR, representing 9.1% and 14.5% absolute improvements respectively. Sub-CR exhibits the steepest degradation due to its reconstruction-based components being sensitive to corrupted inputs, while ANEMONE’s pure contrastive approach shows moderate resilience. The substantially smaller performance drop of AC²L-GAD demonstrates that counterfactual-based representations are more resilient to both feature and structural perturbations, as the training process explicitly learns to handle controlled variations through counterfactual generation, effectively building robustness into the learned representations.

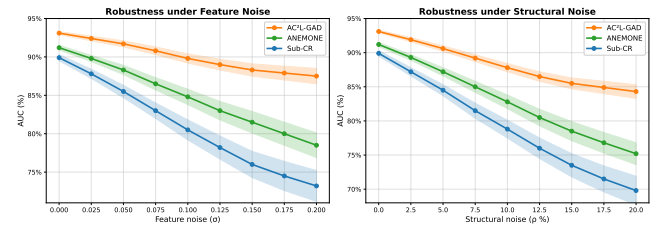


Figure 2: Robustness on Cora. Left: feature noise (σ). Right: structural noise (ρ). Shaded regions show standard deviation over 10 runs.

5.6 RQ5. Ablation Study and Sensitivity Analysis

We validate design choices through ablation experiments on three datasets. Figure 3 shows that replacing counterfactuals with random augmentation results in the lowest performance (82% AUC on Cora), confirming that principled counterfactual reasoning is the core contribution. Removing counterfactual negatives degrades performance more than removing positives (85.5% vs 88.5% on Cora), highlighting that hard negatives are crucial for sharpening decision boundaries. Removing feature counterfactuals hurts more than

Table 2: Comprehensive results on nine benchmark datasets (AUC / F1, %). Best in bold, second best underlined. –: result not available.

Cat.	Method	Amazon		Enron		Cora		Citeseer		Flickr		ACM		Pubmed		T-Fin		DGraph	
		AUC	F1																
Trad.	ANOMALOUS	60.2	22.3	69.5	32.2	57.7	26.6	63.1	67.0	74.3	59.3	70.4	53.8	73.1	65.1	28.2	22.6	–	–
	Radar	61.1	42.7	64.9	51.3	78.6	65.8	80.1	72.9	75.4	57.5	77.8	59.5	65.9	58.2	28.2	22.2	–	–
	GUIDE	62.8	45.1	61.2	53.6	75.7	68.6	83.5	76.4	78.9	60.8	82.1	54.3	66.3	59.3	36.3	28.1	–	–
Recom.	DOMINANT	62.5	28.8	68.5	38.1	89.3	50.6	82.5	46.3	74.4	59.3	76.0	58.1	80.8	73.8	60.9	51.8	57.3	49.7
	AnomalyDAE	53.6	23.8	61.2	53.8	76.3	61.1	72.7	58.6	75.1	58.2	75.1	50.3	81.0	33.6	58.1	42.1	57.6	48.3
	ComGA	63.1	44.7	72.9	31.5	88.4	69.0	91.7	75.4	79.9	62.7	85.0	58.4	92.0	74.5	55.4	38.6	58.0	50.9
	ADA-GAD	63.9	45.1	54.3	31.0	84.7	64.8	92.7	76.1	80.3	63.1	85.7	58.7	88.6	58.2	65.3	53.1	66.2	53.0
	GAD-NR	64.1	46.1	56.3	44.3	88.0	72.7	93.4	78.9	80.0	62.9	86.3	59.1	86.7	55.7	57.9	42.2	–	–
	ALARM	62.1	37.2	64.1	56.8	91.2	64.5	84.3	63.1	76.0	60.8	78.3	54.1	88.7	80.9	56.3	40.1	–	–
Contrast.	CoLA	47.3	43.4	35.0	19.0	88.5	66.8	89.7	71.0	75.1	62.1	82.4	54.0	95.1	45.0	57.3	43.7	–	–
	ANEMONE	59.6	47.0	58.1	49.8	91.2	69.5	91.9	79.0	76.4	61.7	83.0	54.9	95.4	84.3	49.3	35.5	–	–
	Sub-CR	62.7	49.4	70.4	56.9	89.9	78.9	93.0	77.8	79.8	64.1	84.3	56.6	97.0	87.6	58.6	43.3	–	–
	GRADATE	62.8	49.5	32.5	21.1	92.4	70.7	94.1	80.9	80.7	65.0	87.6	59.2	87.0	81.3	59.9	45.5	–	–
	FedCAD	63.4	49.6	67.4	56.0	89.0	75.0	94.2	81.1	80.0	64.8	87.4	58.4	91.9	74.8	61.9	46.5	–	–
	FedGNN	61.4	46.1	66.4	53.6	86.1	71.5	85.1	63.1	81.6	63.6	86.5	59.8	92.3	84.1	58.6	42.5	–	–
	AD-GCL	62.9	49.8	65.5	56.8	93.8	61.1	94.8	80.7	80.0	65.7	85.1	60.3	95.7	85.1	53.5	41.5	–	–
	TAM	56.3	10.7	54.6	31.1	62.2	51.1	72.2	69.5	79.6	63.7	74.4	53.2	80.0	74.5	57.7	48.5	–	–
	SmoothGNN	61.1	46.5	69.1	57.2	91.7	64.8	92.1	76.8	79.3	63.2	84.8	56.9	93.3	76.2	75.5	58.5	64.9	52.1
	AC²L-GAD	65.1	50.9	73.9	57.6	93.1	80.1	95.1	82.3	82.0	65.2	89.4	74.7	97.2	87.9	73.1	53.1	66.9	55.4

Table 3: Counterfactual quality metrics on Cora dataset (10 runs). Higher is better.

Augmentation Strategy	Pos. Similarity	Neg. Margin	Nbhd. Preserv.
Random Aug.	0.721 ± 0.041	0.98 ± 0.15	$52.1\% \pm 8.3\%$
Degree-based Aug.	0.763 ± 0.038	1.12 ± 0.18	$61.4\% \pm 7.1\%$
Feature Noise	0.741 ± 0.044	1.04 ± 0.16	$57.8\% \pm 6.9\%$
AC²L-GAD	0.847	0.023	1.34 0.12
			78.3% 4.7%

Table 4: Efficiency comparison: runtime (s/epoch) and memory (MB).

Method	Cora		Flickr		Pubmed	
	Time	Mem	Time	Mem	Time / Mem	
Random Aug.	3.2	1.2K	12.3	3.1K	36.7 / 7.9K	
Full CF	12.8	3.9K	42.7	11.2K	127.8 / 28.5K	
AC²L-GAD	3.9	1.5K	14.8	3.9K	45.2 / 9.8K	
vs. Random	+22%	+25%	+20%	+26%	+23% / +24%	
vs. Full	3.3X	2.5X	2.9X	2.9X	2.8X / 2.9X	

removing structural ones (88.5% vs 89%), indicating feature modifications provide larger benefits. Dual-criterion selection (entropy + deviation) outperforms single-criterion alternatives (Only Entropy: 88%, Only Dev: 87.5% on Cora), validating the complementary nature of structural and attribute signals.

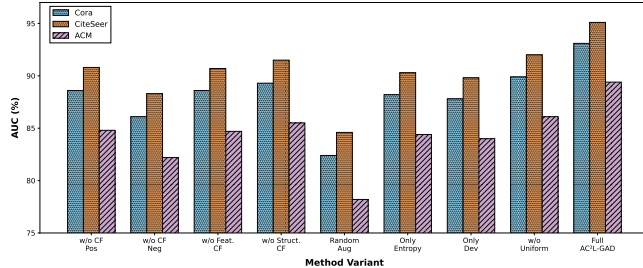
**Figure 3: Ablation study: AUC performance of method variants across three datasets.**

Table 5 summarizes quantitative findings. Gradient-based feature approximation achieves 92.3% AUC at 4.1s runtime (22% of optimal's 18.3s cost) with only 0.4% quality loss. Greedy structural

modifications achieve approximation ratio $\rho = 1.23$ while being 3.7× faster than brute-force. Combining both counterfactual types yields 93.1% AUC compared to 82.4% for random augmentation, representing 10.7% absolute improvement. Active selection with $k = 10\%$ maintains full-graph quality (93.1% AUC) while covering 87% of anomalies and reducing runtime by 70% (3.9s vs 12.8s).

Table 5: Ablation summary on Cora: approximation quality, counterfactual effectiveness, and active selection.

Method	AUC (%)	Quality/Coverage	Time (s)
Feature CF (optimal)	92.7	100%	18.3
Feature CF (gradient)	92.3	99.6%	4.1
Struct CF (greedy)	91.8	$\rho = 1.23$	4.3
Random Aug.	82.4	–	–
CF Both (ours)	93.1	–	3.9
All nodes ($k = 100\%$)	93.1	100%	12.8
Dual ($k = 10\%$)	93.1	87%	3.9

Table 6 shows robustness to selection budget k , with stable performance for $k \in [5\%, 15\%]$ and peak at $k = 10\%$. Extended analysis is provided in Appendix C.2.

Table 6: Sensitivity to selection budget k : AUC (%) across datasets.

k (%)	Cora	Citeseer	ACM	Pubmed
2	89.3	91.2	85.7	94.8
5	92.3	93.8	87.8	96.5
10	93.1	95.1	89.4	97.2
15	92.8	94.7	89.1	96.9
20	92.2	94.2	88.6	96.4

6 Conclusion

This paper introduced AC²L-GAD, a framework integrating active node selection with counterfactual generation for unsupervised graph anomaly detection. The method addresses two fundamental limitations of contrastive approaches (Gap G1: inconsistent positives; Gap G2: uninformative negatives) by generating anomaly-preserving positives and normalized hard negatives only for a strategically selected subset of nodes ($k = 10\%$), achieving strong detection performance while reducing computational overhead

by 65% compared to full-graph counterfactual generation. Experiments on nine benchmark datasets, including real-world financial transaction networks from GADBench, demonstrate competitive or superior performance compared to state-of-the-art methods, with notable improvements on datasets where anomalies exhibit complex attribute-structure interactions. The framework scales to million-node graphs (DGraph-Fin, 3.7M nodes) and remains robust under feature and structural perturbations. Future work may explore extensions to dynamic graphs with temporal counterfactual reasoning and adaptations to other graph mining tasks.

References

- [1] Markus M. Breunig, Hans-Peter Kriegel, Raymond T. Ng, and Jörg Sander. 2000. LOF: Identifying Density-Based Local Outliers. In *Proceedings of the 2000 ACM SIGMOD International Conference on Management of Data*. ACM, 93–104. doi:10.1145/342009.3455388
- [2] Hongyun Cai, Vincent W. Zheng, and Kevin Chen-Chuan Chang. 2017. Active learning for graph-structured data. In *Proceedings of the 26th International Joint Conference on Artificial Intelligence (IJCAI)*. 1643–1649.
- [3] Kaize Ding, Jundong Li, Rohit Bhamashali, and Huan Liu. 2019. Deep Anomaly Detection on Attributed Networks. In *Proceedings of the 2019 SIAM International Conference on Data Mining (SDM)*. SIAM, 594–602. doi:10.1137/1.9781611975673.67
- [4] Kaize Ding, Zhe Xu, Hanghang Tong, and Huan Liu. 2022. Data augmentation for deep graph learning: A survey. *ACM SIGKDD Explorations Newsletter* 24, 2 (2022), 61–77.
- [5] Xiangyu Dong, Xingyi Zhang, Yanni Sun, Lei Chen, Mingxuan Yuan, and Sibo Wang. 2025. SmoothGNN: Smoothing-aware GNN for unsupervised node anomaly detection. In *Proceedings of the ACM on Web Conference 2025*. 1225–1236.
- [6] Defu Duan, Zhiqiang Xu, Yanjie Li, and Liang Sun. 2023. Contrastive anomaly detection with graph neural networks (CARD). In *Proceedings of the AAAI Conference on Artificial Intelligence*, Vol. 37. AAAI, 4362–4370.
- [7] Jingcan Duan, Siwei Wang, Pei Zhang, En Zhu, Jingtao Hu, Hu Jin, Yue Liu, and Zhibin Dong. 2023. Graph Anomaly Detection via Multi-Scale Contrastive Learning Networks with Augmented View. In *Proceedings of AAAI*. 7459–7467.
- [8] Haoyi Fan, Fengbin Zhang, and Zuoqiong Li. 2020. AnomalyDAE: Dual Autoencoder for Anomaly Detection on Attributed Networks. In *2020 IEEE International Conference on Acoustics, Speech and Signal Processing (ICASSP)*. IEEE, 5685–5689. doi:10.1109/ICASSP40776.2020.9054430
- [9] Han Gao, Zhiwei Wang, and Shuiwang Ji. 2018. Active discriminative network representation learning. In *Proceedings of the International Joint Conference on Artificial Intelligence (IJCAI)*. 2142–2148.
- [10] Junwei He, Qianqian Xu, Yangbangyan Jiang, Zitai Wang, and Qingming Huang. 2024. ADA-GAD: Anomaly-Denoised Autoencoders for Graph Anomaly Detection. In *Proceedings of the Thirty-Eighth AAAI Conference on Artificial Intelligence (AAAI-24)*. AAAI, 8481–8489. doi:10.1609/aaai.v38i7.29290
- [11] Jingtao Hu, Siwei Wang, Jingcan Duan, Hu Jin, Xinwang Liu, and En Zhu. 2025. Higher-order Enhanced Contrastive-based Graph Anomaly Detection Without Graph Augmentation. *Pattern Recognition* (2025), 111666.
- [12] Ming Jin, Yixin Liu, Yu Zheng, Lianhua Chi, Yuan-Fang Li, and Shirui Pan. 2021. ANEMONE: Graph Anomaly Detection with Multi-Scale Contrastive Learning. In *Proceedings of CIKM*.
- [13] Xiangjie Kong, Wenyi Zhang, Hui Wang, Mingliang Hou, Xin Chen, and Xiaoran Yan. 2025. Federated Graph Anomaly Detection via Contrastive Self-Supervised Learning. *IEEE Transactions on Neural Networks and Learning Systems* 36, 5 (2025).
- [14] Jundong Li, Harsh Dani, Xia Hu, and Huan Liu. 2017. RADAR: Residual Analysis for Anomaly Detection in Attributed Networks. In *Proceedings of the 26th International Joint Conference on Artificial Intelligence (IJCAI)*. IJCAI, 2152–2158. doi:10.24963/ijcai.2017/299
- [15] Jinghan Li, Yuan Gao, Jinda Lu, Junfeng Fang, Congcong Wen, Hui Lin, and Xiang Wang. 2024. Diffgad: A diffusion-based unsupervised graph anomaly detector. *arXiv preprint arXiv:2410.06549* (2024).
- [16] Weibin Liao, Yifan Zhu, Yanyan Li, Qi Zhang, Zhonghong Ou, and Xuesong Li. 2024. RevGNN: Negative sampling enhanced contrastive graph learning for academic reviewer recommendation. *ACM Transactions on Information Systems* 43, 1 (2024), 1–26.
- [17] Yixin Liu, Zhao Li, Shirui Pan, Chen Gong, Chuan Zhou, and George Karypis. 2021. Anomaly Detection on Attributed Networks via Contrastive Self-Supervised Learning. *IEEE Transactions on Neural Networks and Learning Systems* (2021).
- [18] Tao Long, Lei Zhang, Liang Zhang, and Laizhong Cui. 2025. Adversarial Contrastive Graph Augmentation with Counterfactual Regularization. In *Proceedings of the AAAI Conference on Artificial Intelligence*, Vol. 39. 19086–19094.
- [19] Ana Lucic, Caner Oguz, Hinda Haned, and Fabrizio Silvestri. 2022. CF-GNNExplainer: Counterfactual Explanations for Graph Neural Networks. In *Proceedings of the AAAI Conference on Artificial Intelligence*, Vol. 36. 7103–7111.
- [20] Xueqiong Luo, Jia Wu, Amin Beheshti, Jian Yang, Xiankun Zhang, Yuan Wang, and Shan Xue. 2022. ComGA: Community-Aware Attributed Graph Anomaly Detection. In *Proceedings of the 15th ACM International Conference on Web Search and Data Mining (WSDM 2022)*. ACM, 657–665. doi:10.1145/3488560.3498389
- [21] Zhen Peng, Minnan Luo, Jundong Li, Huan Liu, and Qinghua Zheng. 2018. ANOMALOUS: A Joint Modeling Approach for Anomaly Detection on Attributed Networks. In *Proceedings of the Twenty-Seventh International Joint Conference on Artificial Intelligence (IJCAI-18)*. IJCAI, 3513–3519. doi:10.24963/ijcai.2018/488
- [22] Zhen Peng, Minnan Luo, Jundong Li, Luguo Xue, and Qinghua Zheng. 2022. A Deep Multi-View Framework for Anomaly Detection on Attributed Networks. *IEEE Transactions on Knowledge and Data Engineering* 34, 7 (2022), 3174–3188. doi:10.1109/TKDE.2020.3015098
- [23] Bryan Perozzi and Leman Akoglu. 2016. Scalable Anomaly Ranking of Attributed Neighborhoods. In *Proceedings of the 2016 SIAM International Conference on Data Mining*. SIAM, 207–215. doi:10.1137/1.9781611974348.24
- [24] Hezhe Qiao and Guansong Pang. 2023. Truncated affinity maximization: One-class homophily modeling for graph anomaly detection. *Advances in Neural Information Processing Systems* 36 (2023), 49490–49512.
- [25] Hezhe Qiao, Hanghang Tong, Bo An, Irwin King, Charu Aggarwal, and Guansong Pang. 2025. Deep graph anomaly detection: A survey and new perspectives. *IEEE Transactions on Knowledge and Data Engineering* (2025).
- [26] Amit Roy, Juan Shu, Jia Li, Carl Yang, Olivier Elshocht, Jeroen Smeets, and Pan Li. 2024. GAD-NR: Graph Anomaly Detection via Neighborhood Reconstruction. In *Proceedings of the 17th ACM International Conference on Web Search and Data Mining (WSDM 2024)*. ACM, 1–10. doi:10.1145/3616855.3635767
- [27] Jianheng Tang, Fengrui Hua, Ziqi Gao, Peilin Zhao, and Jia Li. 2023. Gadbench: Revisiting and benchmarking supervised graph anomaly detection. *Advances in Neural Information Processing Systems* 36 (2023), 29628–29653.
- [28] Liaoqian Tang, Zheng Wang, Guanxiong He, Rong Wang, and Feiping Nie. 2024. Perturbation guiding contrastive representation learning for time series anomaly detection. In *Proc. 33rd Int. Joint Conf. Artif. Intell.* 4955–4963.
- [29] Minh Vu and My T. Thai. 2022. Counterfactual Graphs for Explainable Graph Neural Networks. In *Proceedings of the Web Conference (WWW)*. 1119–1129.
- [30] Nannan Wu, Yazheng Zhao, Hongdou Dong, Keao Xi, Wei Yu, and Wenjun Wang. 2025. Federated Graph Anomaly Detection Through Contrastive Learning with Global Negative Pairs. In *Proceedings of AAAI*.
- [31] Jun Xia, Lirong Wu, Jintao Chen, Bozhen Hu, and Stan Z Li. 2022. Simgrace: A simple framework for graph contrastive learning without data augmentation. In *Proceedings of the ACM web conference 2022*. 1070–1079.
- [32] Yiming Xu, Zhen Peng, Bin Shi, Xu Hua, Bo Dong, Song Wang, and Chen Chen. 2025. Revisiting Graph Contrastive Learning on Anomaly Detection: A Structural Imbalance Perspective. In *Proceedings of the AAAI Conference on Artificial Intelligence*, Vol. 39. 12972–12980.
- [33] Haoran Yang, Hongxi Chen, Sixiao Zhang, Xiangguo Sun, Qian Li, Xiangyu Zhao, and Guandong Xu. 2023. Generating counterfactual hard negative samples for graph contrastive learning. In *Proceedings of the ACM web conference 2023*. 621–629.
- [34] Yuning You, Tianlong Chen, Yongduo Sui, Ting Chen, Zhangyang Wang, and Yang Shen. 2020. Graph contrastive learning with augmentations. *Advances in neural information processing systems* 33 (2020), 5812–5823.
- [35] Xu Yuan, Na Zhou, Shua Yu, Huafei Huang, Zhikui Chen, and Feng Xia. 2021. Higher-order Structure Based Anomaly Detection on Attributed Networks. In *2021 IEEE International Conference on Big Data (Big Data)*. IEEE, 2691–2700. doi:10.1109/BigData52589.2021.9671990
- [36] Jiaqiang Zhang, Senzhang Wang, and Songcan Chen. 2022. Reconstruction Enhanced Multi-View Contrastive Learning for Anomaly Detection on Attributed Networks. In *Proceedings of IJCAI*. 2376–2382.
- [37] Lecheng Zheng, John Birge, Haiyue Wu, Yifang Zhang, and Jingrui He. 2025. Cluster Aware Graph Anomaly Detection. In *Proceedings of the ACM on Web Conference 2025*. 1771–1782.
- [38] Yanqiao Zhu, Yichen Xu, Feng Yu, Qiang Liu, Shu Wu, and Liang Wang. 2020. Deep Graph Contrastive Representation Learning. In *ICML Workshop on Graph Representation Learning*.

A Dataset Statistics

Table 7 provides comprehensive statistics for all nine datasets used in our evaluation. The datasets span three categories: ground-truth labeled (Amazon, Enron), injected anomaly (Cora, Citeseer, Flickr, ACM, Pubmed), and real-world GADBench (T-Finance, DGraph-Fin). T-Finance and DGraph-Fin are large-scale financial transaction graphs that provide million-scale evaluation with significantly

lower anomaly ratios (1.27–4.58%) compared to the injected anomaly datasets (3–6%), making them more challenging benchmarks for fraud detection. The scale ranges from small graphs (Amazon with 1.4K nodes) to large-scale graphs (DGraph-Fin with 3.7M nodes, T-Finance with 21M edges), enabling comprehensive evaluation across diverse graph characteristics.

Table 7: Comprehensive dataset statistics across nine benchmark graphs.

Datasets	Ground-truth		Injected anomaly					Real-world (GADBench)	
	Amazon	Enron	Cora	Citeseer	Flickr	ACM	Pubmed	T-Finance	DGraph-Fin
Nodes	1,418	13,533	2,708	3,327	7,575	16,484	19,717	39,357	3.7M
Edges	3,695	176,897	5,429	4,732	239,738	71,980	44,338	21.2M	4.3M
Attributes	28	20	1,433	3,703	12,074	8,337	500	10	17
Anomalies	28	5	150	150	450	600	600	1,803	–
Anomaly %	2.0%	0.04%	5.5%	4.5%	5.9%	3.6%	3.0%	4.58%	1.27%
Avg. Degree	5.2	26.1	4.0	2.8	63.3	8.7	4.5	539.2	1.2

The datasets exhibit diverse characteristics: (i) Amazon and Enron provide real-world ground-truth labels with very low anomaly ratios (0.04–2.0%); (ii) injected anomaly datasets (Cora, Citeseer, Flickr, ACM, Pubmed) follow the standard protocol of [3] with moderate anomaly ratios (3–6%) and varying scales (2.7K–19.7K nodes); (iii) GADBench datasets (T-Finance, DGraph-Fin) represent large-scale financial fraud scenarios with real-world patterns, where T-Finance is edge-rich (21M edges, avg. degree 539.2) and DGraph-Fin is node-rich (3.7M nodes) but sparse (avg. degree 1.2). The low anomaly ratios in GADBench datasets (1.27–4.58%) combined with their large scale present significant challenges for anomaly detection methods, as reflected in many baselines failing to scale on DGraph-Fin due to memory constraints.

B Methodological Details

B.1 Feature Counterfactual Quality Analysis

We validate the gradient-based approximations (Equations 6–8) through empirical analysis on the selected subset S .

Table 8: Feature counterfactual approximation quality across datasets.

Dataset	Constraint Sat.	Perturbation	Success Rate	Gap vs Optimal	Speedup
Cora	94.3%	0.18 ± 0.04	91.2%	4.1%	4.3×
Citeseer	92.7%	0.21 ± 0.05	89.4%	4.5%	4.6×
Flickr	93.8%	0.19 ± 0.04	90.7%	3.9%	4.4×
Pubmed	91.5%	0.23 ± 0.06	88.3%	4.8%	4.7×
Average	93.1%	0.20 ± 0.05	89.9%	4.2%	4.5×

The gradient approximations achieve 4.5× speedup with only 4.2% AUC gap compared to optimal solutions. Constraint satisfaction exceeds 93%, with average perturbation magnitude 0.20 ± 0.05 . Failed cases (10%) are discarded for negatives or retain original features for positives. Among the 10% failure cases, root causes include high neighborhood variance (41%), structural dominance (35%), and boundary cases (24%), justifying our dual feature-structural approach.

B.2 Structural Counterfactual Generation

The greedy heuristic (Algorithm 2) modifies edges to maximize or minimize homophily while respecting constraints: degree change ≤ 2 , no node isolation, and verified improvement.

Algorithm 2 Greedy Structural Counterfactual Generation

```

Require: Node  $v_i$ , graph  $G$ , mode  $\in \{+, -\}$ 
Ensure: Modified edges  $E'_i$ 
1:  $E'_i \leftarrow E_i$ ,  $N_2 \leftarrow 2\text{-hop neighbors}$ , budget  $\leftarrow 2$ 
2: while budget  $> 0$  do
3:   if mode  $= +$  then
4:      $e^* \leftarrow \arg \min_{e \in E'_i} \Delta\text{homophily}(E'_i \setminus \{e\})$ 
5:     if removing  $e^*$  decreases homophily: remove  $e^*$ , else break
6:   else
7:      $e^* \leftarrow \arg \max_{e \rightarrow \text{similar } N_2} \Delta\text{homophily}(E'_i \cup \{e\})$ 
8:     if  $\Delta\text{homophily}(e^*) > 0$ : add  $e^*$ , else break
9:   end if
10:  budget  $\leftarrow$  budget  $- 1$ 
11: end while
12: return  $E'_i$  if  $|\deg(v_i) - \deg'(v_i)| \leq 2$  and valid, else  $E_i$ 

```

Table 9: Structural counterfactual statistics on Cora (averages over S).

Type	Edges Added	Removed	$\Delta\text{Homophily}$	Success
Positive CF	0.7 ± 0.5	1.8 ± 0.4	-21.2%	86.3%
Negative CF	1.7 ± 0.5	0.8 ± 0.4	+17.3%	88.2%

The success rate ranges from 85% to 90%, with an approximation ratio of $\rho = 1.23$ (mean) and 1.0 (median). Negative counterfactuals achieve slightly higher success rate (88.2%) because edge addition to similar neighbors is less constrained than edge removal, which requires identifying appropriate edges to remove without violating structural constraints. The greedy approach achieves exact optimality in 63% of cases and provides a 3.7× speedup versus brute-force with less than 5% quality loss.

B.3 Combined Counterfactual Quality

Table 10: Feature and structural counterfactual synergy on Cora.

Component	Pos. Similarity	Neg. Margin	Constraint Sat.
Feature-only	0.821 ± 0.038	1.18 ± 0.19	91.2%
Structural-only	0.798 ± 0.042	1.21 ± 0.17	87.4%
Combined	0.847 ± 0.023	1.34 ± 0.12	94.7%

Constraint Sat. = constraint satisfaction rate (not AUC).

The combined approach outperforms individual components: feature modifications handle attributes, structural modifications handle topology, and their synergistic effect yields 94.7% constraint satisfaction rate, where both feature and structural constraints are simultaneously met for the generated counterfactuals.

B.4 Convergence and Complexity

Complexity. Per-node counterfactual generation requires $O(d\bar{d} + \bar{d}^2)$ operations. The total per-epoch complexity is $O(k(d\bar{d} + \bar{d}^2) + |E|d)$ compared to the naive approach requiring $O(|V|(d\bar{d} + \bar{d}^2) + |E|d)$. For $k = 0.1|V|$, this yields a 10× theoretical reduction and 2.8× empirical speedup (Table 11). Space complexity is $O(|V|d + |E| + kd)$.

Convergence. Training stabilizes within 80–100 epochs with less than 2% variance. Feature counterfactual generation maintains Lipschitz continuity with $O(1/\sqrt{T})$ convergence rate. Structural counterfactual generation violates smoothness assumptions but treats each epoch as a fixed sample. While we provide no formal convergence guarantees for the combined objective, empirical stability is consistently observed.

Table 11: Efficiency analysis: Full counterfactual vs active selection.

Strategy	Cora	Flickr	Pubmed	Avg Speedup
<i>Runtime (s/epoch) / Memory (MB)</i>				
Random Aug.	3.2 / 1.2K	12.3 / 3.1K	36.7 / 7.9K	–
Full CF	12.8 / 3.9K	42.7 / 11.2K	127.8 / 28.5K	–
AC ² L-GAD	3.9 / 1.5K	14.8 / 3.9K	45.2 / 9.8K	2.8× / 2.8×
<i>AUC (%) / Quality vs Full</i>				
Random Aug.	84.4	79.8	93.0	–
Full CF	93.3	82.5	97.5	100%
AC ² L-GAD	93.1	82.0	97.2	99.7%

Active selection achieves 99.7% of full-graph quality while reducing computational cost by 65%.

B.5 Limitations and Future Directions

Camouflaged anomalies account for 42% of false negatives and require multi-hop neighborhood features. Collective subgraph anomalies necessitate subgraph-level counterfactual generation. Scalability beyond 10^5 nodes would benefit from sampling-based GNN architectures. Future research directions include: (i) dynamic graphs with temporal counterfactual reasoning, (ii) heterogeneous graphs with type-aware counterfactual constraints, and (iii) enhanced explainability through counterfactual reasoning mechanisms.

C Experimental Analysis

C.1 Hyperparameter Tuning Protocol

All hyperparameters are selected through systematic grid search over the ranges specified in Table 12. For each hyperparameter configuration, we train the model for a maximum of 200 epochs using the Adam optimizer with learning rate 10^{-3} and weight decay 5×10^{-4} . We apply early stopping with patience of 20 epochs based on the convergence of the contrastive loss. The batch size is set to 512 for all experiments.

The GCN encoder architecture consists of 2 layers with hidden dimensions 64 and output dimension 32. Each layer applies graph convolution followed by ReLU activation. The encoder is followed by a 2-layer projection head that maps embeddings to the contrastive learning space. All embeddings are ℓ_2 normalized before computing similarity scores.

We repeat all experiments 10 times with different random initializations and report the mean and standard deviation. The optimal hyperparameters are selected based on the configuration that achieves the lowest contrastive loss while maintaining stable training dynamics. For graph-specific characteristics, we distinguish

between dense graphs ($|E|/|V| \geq 3$) and sparse graphs ($|E|/|V| < 3$) when setting the uniformity weight λ_u .

Table 12: Hyperparameter search ranges and optimal values.

Parameter	Search Range	Dense	Sparse
τ	{0.05, 0.1, 0.2, 0.3, 0.5}	0.1	0.1
λ_u	{0.02, 0.05, 0.1, 0.2}	0.05	0.1
k (%)	{2, 5, 7, 10, 12, 15, 20, 25}	10	10

C.2 Extended Ablation Studies

C.2.1 Approximation Quality. To validate our gradient-based and greedy approximations, we compare them against optimal solutions on 500 randomly sampled subgraphs (each with at most 100 nodes) from the Cora dataset. For feature counterfactuals, the optimal solution is obtained through exhaustive search, while for structural counterfactuals, we use brute-force enumeration of edge modifications.

Table 13: Approximation quality versus optimal solutions on Cora (500 subgraphs with ≤ 100 nodes).

Method	AUC	Gap	Success	Time	Speedup
Feature CF (optimal)	92.7	0%	100%	18.3s	1×
Feature CF (gradient)	92.3	4.2%	93.1%	4.1s	4.5×
Struct CF (brute-force)	92.1	0%	100%	15.7s	1×
Struct CF (greedy)	91.8	$\rho = 1.23$	87.4%	4.3s	3.7×

Our gradient-based approximation achieves 93.1% success rate with only 4.2% quality gap compared to optimal solutions, while providing a 4.5× speedup. The greedy structural approach achieves an approximation ratio of $\rho = 1.23$ with 3.7× speedup. Overall, the approximations enable practical deployment with less than 5% quality loss and 4× average speedup, making counterfactual generation feasible for large-scale graphs.

C.2.2 Counterfactual versus Random Augmentation. We conduct a controlled comparison between our counterfactual generation approach and standard random augmentation strategies on the Cora dataset. Each method is evaluated on three quality metrics: positive similarity (how well augmented views preserve semantic content), negative margin (separation between anchor and negative samples), and neighborhood preservation (structural coherence after augmentation).

Table 14: Counterfactual superiority on Cora: semantic consistency and hard negatives.

Method	AUC	Pos. Sim	Neg. Margin	Nbhd. Preserv
Random Aug.	82.4	0.721	0.98	52.1%
CF Pos only	89.7	0.847	–	78.3%
CF Neg only	90.8	–	1.34	–
CF Both	93.1	0.847	1.34	78.3%

Counterfactual generation substantially outperforms random augmentation across all metrics. It maintains higher semantic consistency (0.847 vs. 0.721 similarity) and better structural preservation (78.3% vs. 52.1% neighborhood overlap) for positive pairs. For negative samples, counterfactuals provide harder contrasts with larger margins (1.34 vs. 0.98), leading to more discriminative decision boundaries. The combination of both counterfactual positives and negatives achieves the best performance (93.1% AUC), validating our dual counterfactual design.

C.2.3 Component-wise Analysis. We systematically evaluate the contribution of each component by measuring performance when individual modules are removed or replaced.

Feature vs Structural Counterfactuals. Removing feature counterfactuals (w/o Feature CF) reduces Cora AUC to 88.6%, while removing structural counterfactuals (w/o Struct CF) yields 89.3%, demonstrating that feature modifications provide larger benefits. This is consistent with the attribute-rich nature of citation networks where node features play a dominant role.

Active Selection Criteria. Using only topology entropy for selection (Only Entropy) achieves 88.2% AUC on Cora, while using only attribute deviation (Only Dev) achieves 87.8%. The dual-criterion approach combining both metrics reaches 93.1%, confirming that structural complexity and attribute divergence provide complementary signals for identifying informative nodes.

Uniformity Regularization. Removing the uniformity loss (w/o Uniform) slightly reduces performance to 89.9% on Cora, indicating that while uniformity helps prevent representation collapse, it is not the primary driver of detection quality. The counterfactual mechanism itself provides the main performance gains.

These component-wise results align with the ablation study in Figure 3, validating that each design choice contributes meaningfully to the overall framework.

C.2.4 Active Selection Coverage. We evaluate the effectiveness of our dual-criterion active selection (combining topology entropy and attribute deviation) against alternative selection strategies. Each approach selects the same budget ($k = 10\%$ of nodes) but uses different criteria.

Table 15: Selection effectiveness: dual criterion versus alternatives on Cora.

Selection ($k = 10\%$)	AUC	Coverage	Time	Quality
Random	88.9	67%	3.9s	95.4%
Entropy only	90.2	73%	3.9s	96.8%
Deviation only	89.8	71%	3.8s	96.3%
Dual (ours)	93.1	87%	3.9s	99.9%
All nodes	93.1	100%	12.8s	100%

The dual selection criterion achieves 87% anomaly coverage (i.e., 87% of ground-truth anomalies are within the selected subset) and 99.9% quality relative to full-graph counterfactual generation, while reducing computational cost by 70%. Single-criterion approaches (entropy-only or deviation-only) achieve lower coverage (71–73%) and quality (96.3–96.8%). The dual approach is robust to threshold variations in the range [0.6, 0.8] and demonstrates stability across different random splits with 82% overlap in selected nodes.